Artificial Organs
••(••):••–••, Wiley Periodicals, Inc.

Investigation of the Washout Effect in a Magnetically Driven Axial Blood Pump

*Michael Triep, *Christoph Brücker, †Wolfgang Kerkhoffs, †Oliver Schumacher, and †Oliver Marseille

**Institut für Mechanik und Fluiddynamik, TU Bergakademie Freiberg, and †CiruLite Inc., Aachen, Germany*

Abstract: For a long-term implementation of the magnetically driven CircuLite blood pump system, it is extremely important to be able to ensure a minimum washout flow in order to avoid dangerous stagnation regions in the gap between the impeller and the motor casing as well as near the pivot–axle area at the holes in the impeller's hub. In general, stagnation zones are prone to thrombus formation. Here, the optimal impeller/motor gap width will be determined and the washout flow for different working conditions will be quantitatively calculated. The driving force for this secondary flow is mainly the strong pressure difference between both ends of the gap. Computational fluid dynamics (CFD) and digital particle image velocimetry (DPIV) will be used for this analysis. **Key Words:** Axial blood pump—Sealless—Magnet drive—Computational fluid dynamics—Digital particle image velocimetry—Washout flow.

The design of miniature rotary blood pumps is often based on established pump concepts from classical turbomachinery. However, key aspects like the different medium and flow regime have to be considered in the early design stage for the success especially of blood pump systems for long-term applications. Classical impellers are driven through a sealed shaft by an electric motor. The interface between moving and fixed parts is always a critical region in rotary blood pumps, because shear strain becomes locally very high. This leads to a higher blood traumatization close to the shaft in the axial impeller–motor gap, and potentially to thrombus formation, which should be prevented in any operating case of the pump. This problem can be circumvented by the use of a fixed axle with an axial pivot bearing on top of it inside the impeller body and the impeller being driven magnetically (1,2). In combination with two washout holes in the impeller's hub, thrombus formation can thus be avoided at the nonrotating/rotating interface (3). This concept is used by CircuLite (Saddle Brook, NJ, USA) for an implantable long-term microaxial blood pump that connects the left atrium with the arteria subclavia (Fig. 1).

The main goal of the present investigation is the study and optimization of the induced washout flow through the axial impeller–rotor gap and the radial impeller–axle gap in order to avoid stagnation zones near the axle pivot during all operation conditions of the CircuLite pump.

Both numerical (computational fluid dynamics [CFD]) and experimental (digital particle image velocimetry [DPIV]) methods are used complementarily. Washout-flow efficiency in the impeller could be improved through variation of the axial gap widths.

MATERIALS AND METHODS

The MicroVad pump

The two-bladed CircuLite impeller was incorporated into the MicroVad pump system. Blood was sucked through an inflow cannula by the impeller, which has a blade tip diameter of 6.6 mm. The flow was redirected by the blades into the annular channel

doi:10.1111/j.1525-1594.2008.00630.x

Received February 2008; revised June 2008.
Address correspondence and reprint requests to Dr. Michael Triep, TU Bergakademie Freiberg—Institut für Mechanik und Fluiddynamik, Lampadiusstr. 4 Freiberg 09596, Germany. E-mail: Michael.Triep@imfd.tu-freiberg.de
Presented in part at the 15th Congress of the International Society for Rotary Blood Pumps held on November 2–4, 2007 in Sydney, Australia.

JOBNAME: No Job Name PAGE: 2 SESS: 20 OUTPUT: Tue Sep 2 16:41:29 2008
/v2503/blackwell/journals/aor_v32_i10/aor_630

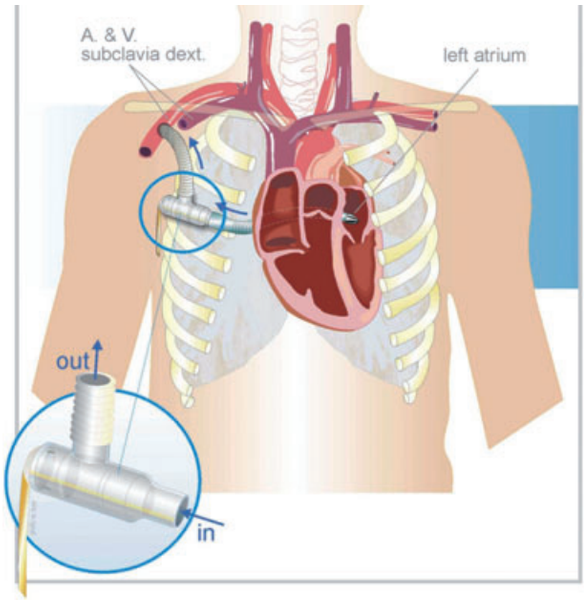

Colour

FIG. 1. Implementation of the MicroVad pump system into the left atrium.

between the electric motor and the casing, and was delivered tangentially into the outlet graft. The system reached at physiological conditions a discharge rate of 3.5 L/min and may be operated at a maximum rotational speed of 28.000 rpm. The power consumption was in the order of 6–9 W.

The impeller was driven magnetically so that no sealing is needed. It was mounted on top of a fixed cylindrical axle, thereby forming a constant radial gap as shown in Fig. 2. In combination with the rotor/motor gap and two holes in the impeller's hub, a washout channel was created. During operation of the pump, a bypass flow through this washout channel was induced so that thrombus formation at the critical ball pivot is prevented.

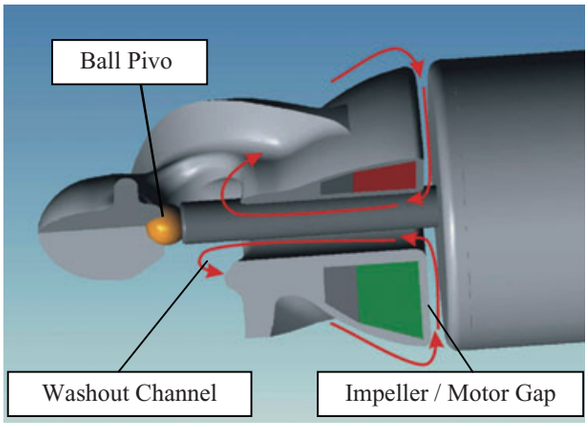

Colour

FIG. 2. Induction of the washout flow.

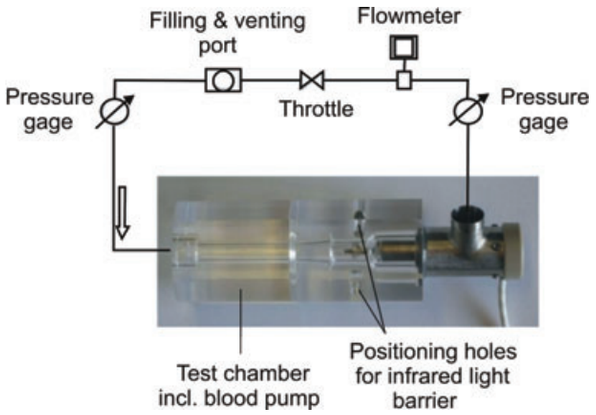

Colour

FIG. 3. Flow circuit for pump tests.

Experimental flow circuit

For the purpose of the study of the overall performance of the pump, in particular the visualization of the washout flow, the impeller was integrated into a hydraulic mock loop (Fig. 3).

A major feature of the setup is the fully transparent Perspex housing of the pump, which allows full optical accessibility into the inlet cannula, the impeller, and the motor region of the main flow. The test chamber is an identical copy of the real clinical pump device. A Newtonian test fluid composed of water/glycerine mixture (35 weight percent glycerine) with a density of 1060 kg/m^3 and a dynamic viscosity of 3.6 cP was used as working fluid. The pressure load and flow was regulated by a throttle valve downstream of the pump, and the flow rate was measured by an ultrasound flowmeter. The connector of the impeller to the mock circuit allows an easy exchange of similar impeller types with small geometric parameter changes.

DPIV setup

Detailed measurements of the internal flow within the pump were carried out using DPIV. This method allows in principle to determine the planar flow field in a selected plane of the flow. Therefore, the laser beam of a phase-triggered double-pulse Nd:Yag laser (Photonics, Edinburgh, UK) with a power of 30 mJ/pulse and a wavelength of 532 nm was expanded and focused to a 0.2-mm light sheet. A prism system redirected the sheet from top and bottom into the test chamber. A micropositioning stage allows to move

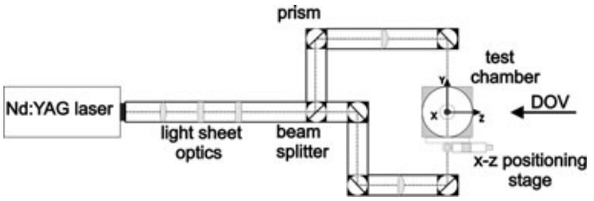

FIG. 4. Optical arrangement (direction of view [DOV]) (4–6).

the whole test chamber through the light sheet. The full optical arrangement can be seen in Fig. 4.

The flow was seeded with small fluorescent tracer particles (Dantec Dynamics A/S, Skovlunde, Denmark) with a mean diameter of 5 µ in a concentration of 0.6 g/L. The fluorescent light of the particles passed an orange filter (LOT-Oriel GmbH & Co. KG, Darmstadt, Germany), whereas disturbing reflections were cut off. A telecentric lens (SILL Optics GmbH & Co. KG, Wendelstein, Germany) with a fixed magnification of 1.422 was used in combination with a CCD sensor (1280×1024 pixels, double-shutter, Sensicam PCO AG, Kelheim, Germany) to record the particle images in the light sheet. Measurements were taken in the axial centerplane and in planes with axial offset. An infrared light barrier allows to synchronize the laser pulse to any desired angular phase position of the impeller electronically. A Labview controller console in combination with a counter card (National Instruments, Austin, TX, USA) was used for phase-locked recording. The pulse separation was 10 µs. Velocity fields were calculated with our own custom routines by cross-correlation procedure with window shifting and window refinement technique. The particle density was high enough to achieve high-quality vector fields with 32×32 interrogation areas (7). The final results represent averages of 50 DPIV recordings at the same phase position. The velocity data were used for direct comparison with the results from the numerical simulation.

Numerical setup

The numerical flow simulations of the pump allow visualizing flow regions that are difficult to access by experimental methods such as the radial gap part of the bypass (washout) channel. Furthermore, they enable to show distributions, for example, of the wall shear stress or pressure in order to identify hot spots, and most important for the present work, the exact determination of integral quantities like the net washout flow and the average pressures in predefined sections of the flow field.

In the present study, the three-dimensional CAD model of the blood pump system is transferred into a computational structured multiblock grid using a grid generation tool (ANSYS ICEM CFD 10.0, ANSYS, Inc., Canonsburg, PA, USA). The computational domain as marked in Fig. 5 includes the extended inflow region, the impeller, and the downstream annular flow channel.

Special attention was paid to the meshing of the washout holes. Refinements toward near-wall regions and especially a fine discretization in blade and gap regions were taken into consideration. The grid consists in total of 2.65 million hexahedral cells. The numerical flow simulation was performed using the commercial CFD software STAR-CD (Computational Dynamics Limited, London, UK). The code numerically solves the conservation equations of mass and momentum by means of a finite volume approach. The Reynolds number based on the interior diameter of the pump casing $D_{ref} = 6.8$ mm reaches values dependent on the working point of about 2875. Therefore, turbulent flow is taken into account by a Reynolds averaged approach and the low-Reynolds k-ε turbulence model. A major advantage of this model is its treatment of the near-wall region. Blood was treated as a single-phase, incompressible, isothermal (37°C) Newtonian fluid with constant density (1060 kg/m^3) and viscosity (3.6 cP). Boundary conditions were chosen in agreement with the experimental situation described in the section before and are defined as follows: a fully developed turbulent velocity profile is set at the entrance of the inflow cannula. Due to the incompressible character of the fluid, the pressure was set in average constant in the outlet of the test compartment, so that the simulated relative pressure field can be transferred in the postprocessing to the correct pressure level with

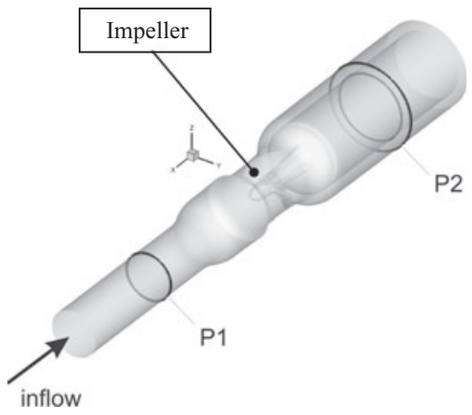

FIG. 5. Domain of computation.

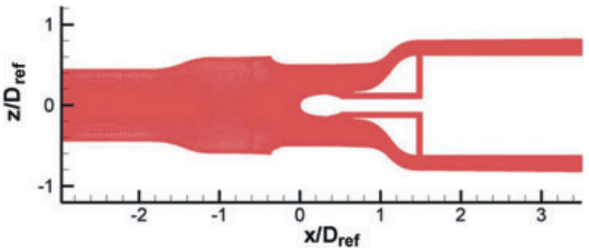

FIG. 6. Side view of the region of interest.

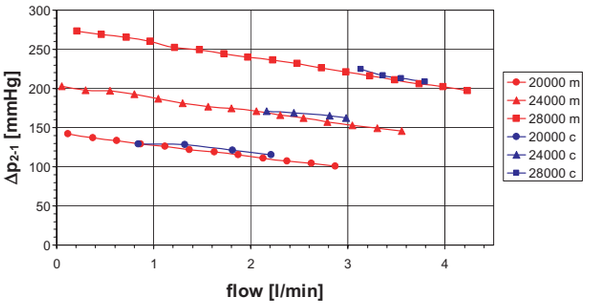

FIG. 7. Comparison of flow curves: measured (m) and computed (c).

the help of experimental measurements. The simulations were carried out on a static grid with additional source terms due to rotation in the conservation equations, which turned out to be very adequate for the purpose of this study. The stagnation point at the tip of the rotor's hub is defined as the origin of the coordinate system as shown in Fig. 6. Position P1 (see Fig. 5) is located 2.95 D_{ref} in front of the origin, and position P2 is located 3.5 D_{ref} behind the origin. The x–z plane is defined here as the plane perpendicular to the washout hole.

RESULTS

The results are structured as follows: first, the simulated operating points are compared against measured performance curves and are discussed, then, the washout flow is determined and analyzed in more detail for different impeller/motor gap widths, the computed general flow field is described and compared with experimental data, and finally, the liftoff force and minimum static pressure are derived.

Flow curves

The chosen working points for simulations were extracted from hydraulically measured performance curves obtained over the whole clinical pump system. The overall pressure differences were varied from 60 to 120 mm Hg, the rotational speeds from 20 000 to 28 000 rpm. The gap between the impeller and the motor was 400-μ wide. The comparison of the analyzed working points within the operating envelope of the pump is shown in Fig. 7. Red and blue denote measured and computed values, respectively. The pressure heads in the curves of Fig. 7 were obtained experimentally and numerically from the average pressures acting in sections close to the impeller P1 and P2 as introduced in Fig. 5 for direct comparison. The curves show good agreement.

A useful way to compare all cases is to nondimensionalize the pressure head Δp_{P1-P2} between positions P1 and P2 from Fig. 5 and the volume flow Q in the following way:

$$\text{Head coefficient:} \quad \psi = \frac{\Delta p_{P2-P1}}{\frac{1}{2}\rho u_{tip}^2}$$

$$\text{Flow coefficient:} \quad \varphi = \frac{Q}{\frac{\pi}{4} d_{tip}^2 u_{tip}}$$

where $\frac{1}{2}\rho u_{tip}^2$ means a fictitious dynamic pressure, and $\frac{\pi}{4} d_{tip}^2 u_{tip}$ a fictitious volume flow based on the blade tip speed, $u_{tip} = \pi n d_{tip}$, and the blade tip diameter, d_{tip}. The diagram in Fig. 8 confirms the expected overlapping of the curves corresponding to different rotational speeds n as in turbomachinery theory (8).

Washout flow

The washout flow acts as a bypass that permits recirculation of the blood when a certain bypass pressure difference between both ends of the washout channel (dependent on the rotational speed of the impeller) is reached. In this section, the axial gap between the impeller and the motor will be varied from 400 to 600 μ as shown in Fig. 9.

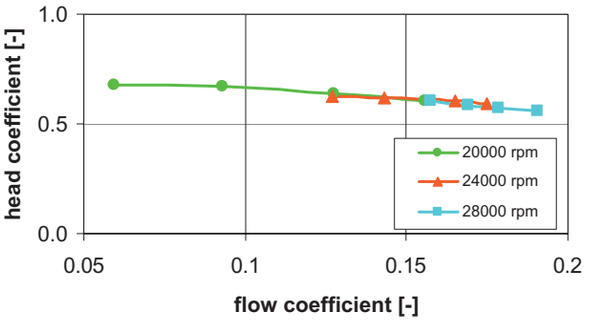

FIG. 8. Dimensionless flow chart.

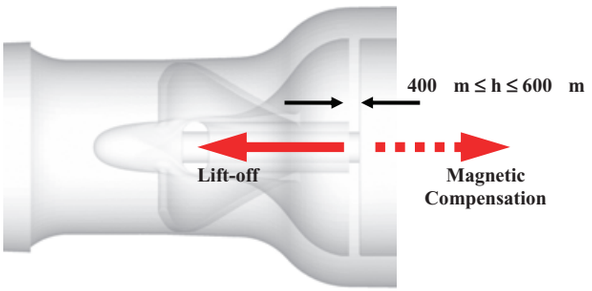

FIG. 9. Washout gap geometry variation and net force direction.

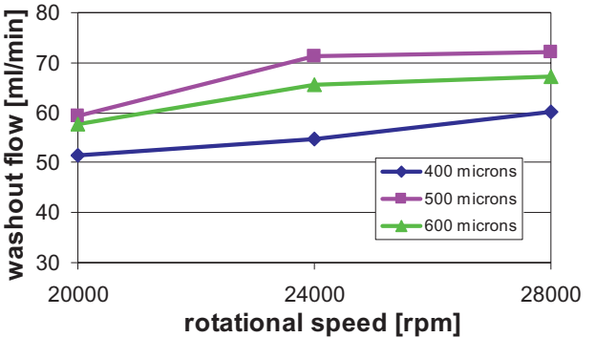

FIG. 10. Washout flow at different rotational speeds and axial gap widths; overall pressure head $\Delta p = 80$ mm Hg.

The upper limit of 600 µ ensures sufficient magnetic attraction, which prevents the impeller to lift off. The net liftoff force is the sum of all fluiddynamic forces acting onto the impeller's surface, for example, the pressure and viscous forces. In order to avoid a damaging physical contact between the impeller and the motor at possible tumbling instabilities of the rotor before reaching the actual working point, the lowest tolerable axial gap width is set to 400 µ.

In general, the washout flow is a function of the channel geometry as well as of the operation conditions such as the rotational speed and the pressure head across the pump. Figure 10 shows the washout flow results obtained for three different axial gap widths at an overall pressure head of $\Delta p = 80$ mm Hg. A gap width of 500 µ evidenced the highest washout flow for all working conditions considered.

On the one hand, for a wider gap, the pressure loss becomes higher due to secondary flows; on the other hand, for a smaller gap width, the pressure loss gets higher due to friction. In effect, a trade-off between these two tendencies leads to the optimal gap width of 500 µ.

In Fig. 11, the whole flow field in a plane through the washout hole and in a perpendicular plane in the impeller region is shown. The streamlines show the existence of a stagnation region near the pivot (see also Fig. 2).

The tip leakage vortex, a back-flow region at the impeller housing, and the secondary flow in the axial gap between the impeller and the motor are also visualized. In addition, the plots include the relative pressure distributions, which are color coded according to the color map. The reference pressure for the CFD simulations was the atmospheric pressure of 750 mm Hg, which was held constant at the outlet boundary. The driving pressure difference for the washout flow can be deduced from the plots.

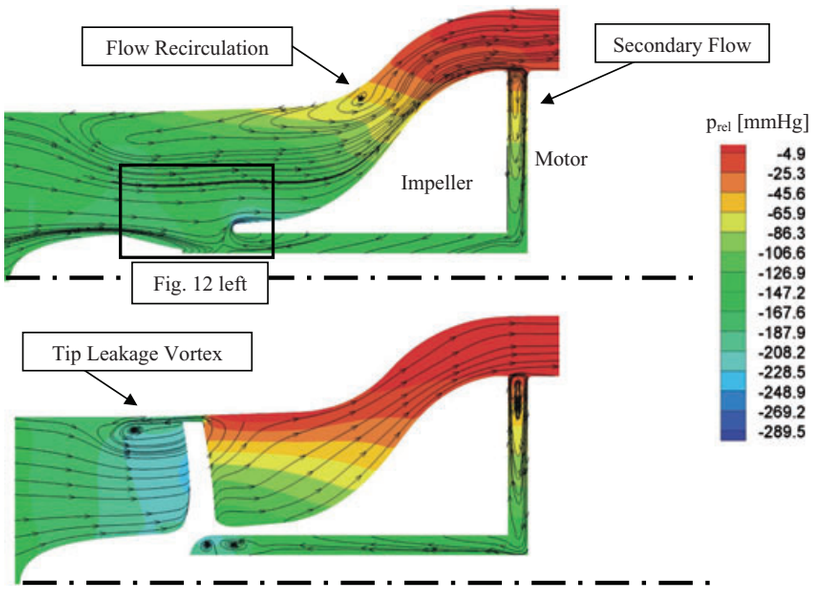

FIG. 11. Sectional streamlines pattern and pressure distribution in the impeller region for working condition: $n = 24\,000$ rpm, $Q = 2.81$ L/min, $\Delta p = 80$ mm Hg.

JOBNAME: No Job Name PAGE: 6 SESS: 20 OUTPUT: Tue Sep 2 16:41:29 2008
/v2503/blackwell/journals/aor_v32_i10/aor_630

Colour

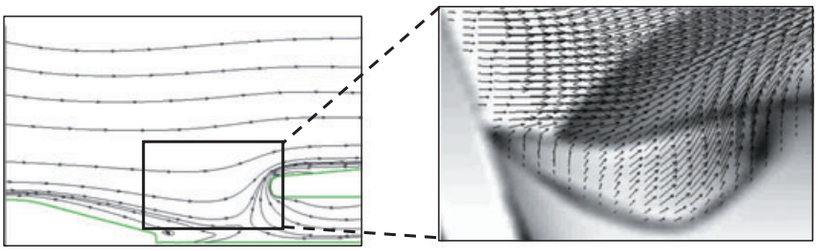

FIG. 12. Washout flow visualization for working conditions: $n = 24\,000$ rpm, $Q = 2.81$ L/min, $\Delta p = 80$ mm Hg; streamlines CFD (left), velocity vectors DPIV (right).

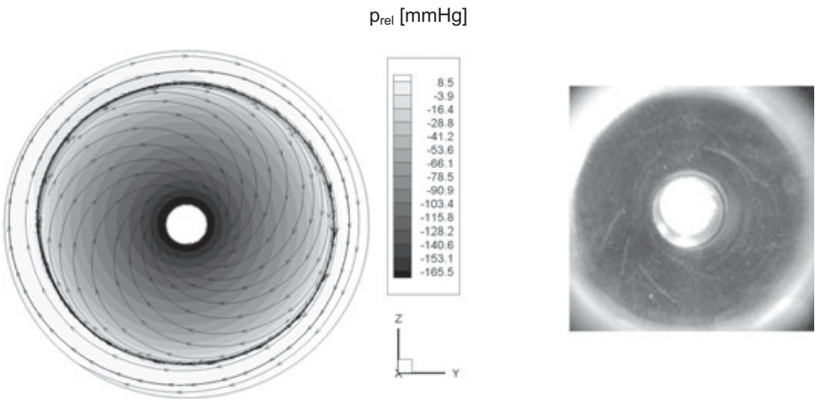

FIG. 13. Flow and pressure distribution in the axial gap between impeller and motor; comparison of numerical simulation (left) and experiment (right): streamlines (left, $\Delta p = 120$ mm Hg, $n = 24\,000$ rpm, $Q = 2.1$ L/min) versus particle traces (right, $\Delta p = 135$ mm Hg, $n = 24\,000$ rpm, $Q = 1.8$ L/min).

Comparison CFD to DPIV

Figure 12 shows a comparison between numerical simulation and experiment of the flow field in the washout hole region. The streamlines (left) and the velocity vectors (right) evidence the path of the mass leaving the radial gap through the washout hole. The bypass flow is sharply turned in downstream direction by the oncoming main flow, indicating that the major part leaves the hole at the trailing edge.

Figure 13 highlights the inward direction of the flow in an axial section plane near the front end of the motor. The slope of the paths of the particle traces (3) agrees well with the slope of the streamlines.

Liftoff force and minimum static pressure

From the numerical simulations, we were further able to calculate the net liftoff force and to localize low-pressure regions. For an overall pressure head of $\Delta p = 80$ mm Hg and a flow of 2.81 L/min at 24 000 rpm, the liftoff force is 0.38 N. The MicroVad blood pump system is designed to operate without any risk of cavitation within the operational envelope. To obtain the absolute pressure field p_{abs}, the computed absolute pressure level $p_{comp,abs}$ is adapted according to the experimental pressure $p_{exp,P1}$ and the computed pressure $p_{comp,P1}$ at position P1 as follows: $p_{abs} = p_{comp,abs} + (p_{exp,P1} - p_{comp,P1})$.

The results of the CFD study showed that the lowest static pressure is 333.8 mm Hg at the operating point of 28.000 rpm and 60 mm Hg. This highest depression occurs at the suction side of the blades near the leading edge (Fig. 14). The volume- and area-based distributions of the pressure in the impeller region for this specific case are given in Fig. 15. They indicate that cavitation will not occur, when assuming a vapor pressure of 47 mm Hg for blood as given by Chambers et al. (9). The present assist device is an intracorporeal blood pump, so that nuclei size distributions and concentrations in the blood are not likely to differ from those encountered in vivo.

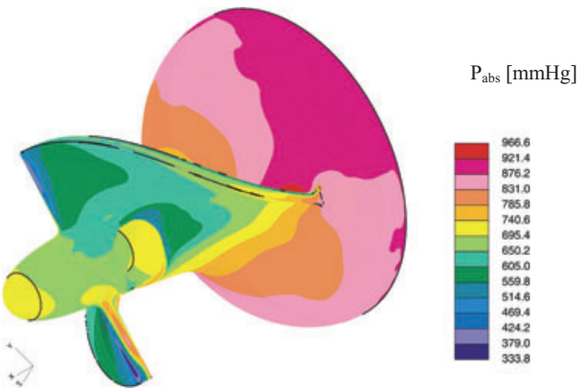

Colour

FIG. 14. Pressure distribution on the impeller for $n = 28.000$ rpm and $\Delta p = 60$ mm Hg.

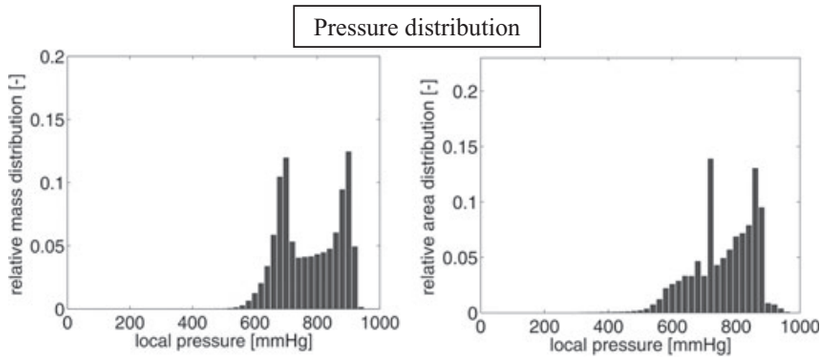

FIG. 15. Volume- (left) and area (right)-based distributions of pressure for $n =$ 28.000 rpm and $\Delta p = 60$ mm Hg.

DISCUSSION AND CONCLUSION

The main goal of the present investigation was the study and optimization of the induced washout flow through the axial impeller–motor gap and the radial impeller–axle gap in order to avoid thrombus formation during all operation conditions of the sealless CircuLite pump. Steady-state, three-dimensional turbulent simulations and DPIV measurements were carried out for various working conditions. The results obtained via the CFD simulations are in a good qualitative and quantitative agreement with the DPIV measurements. The washout flow is maximized with the axial impeller–motor gap at 500 µ. An increase of the free cross-section of the gap leads to a decrease of the pressure loss and therefore to an increase of the washout flow. The washout channel acts as a classical bypass in pumping systems. Therefore, any increase in the bypass flow (washout) counteracts to the pressure load and net flow rate at the working point.

Furthermore, the liftoff force obtained via CFD is well below the value for the magnetic attraction given by Kerkhoffs et al. (3), and the minimum static pressure emerging in the pump is well above the vapor pressure of blood of 47 mm Hg.

In the next step, continued iterative geometric adaptations for an even better washout effect at physiological pressure loads will be considered. It is important to include the study of fluid residence time and the effectiveness of the mass exchange in the front part of the pivot.

In addition, the mechanical stability of the pump will be studied, in particular, the restoring moment from the pressure acting on the impeller's surface. In effect, a trade-off of the mechanical stability, on the one hand, and a good washout effect, on the other hand, has to be established.

REFERENCES

1. Havlik R, Kerkhoffs W, Jiao L, Schumacher O, Reul H, Habib N. Intravascular micropump for augmented liver perfusion: first in vivo experience. *Artif Organs* 2001;25:392–4.
2. Mahmood A, Kerkhoffs W, Schumacher O, Reul H. Investigation of materials for blood-immersed bearings in a microaxial blood pump. *Artif Organs* 2003;27:169–73.
3. Kerkhoffs W, Schumacher O, Meyns B, et al. Design, development, and first in vivo results of an implantable ventricular assist device, MicroVad. *Artif Organs* 2004;28:904–10.
4. Brücker C, Schröder W, Apel J, Reul H, Siess T. DPIV study of the flow in a microaxial blood pump. *Proceedings of the 9th Symposium on Transport Phenomena and Dynamics of Rotating Machinery. ISROMAC-9.* Honolulu, HI, 2002.
5. Triep M, Brücker C, Schröder W, Siess T. Computational fluid dynamics and digital particle image velocimetry study of the flow through an optimized micro-axial blood pump. *Artif Organs* 2006:30:384–91.
6. Triep M, Brücker C, Siess T. DPIV-measurements of the flow field in a micro-axial blood pump. *Proceedings of the 13th Symposium on Applications of Laser Techniques to Fluid Mechanics*. Lisbon, 2006.
7. Adrian R. Particle-imaging techniques for experimental fluid mechanics. *Ann Rev Fluid Mech* 1991;23:261–301.
8. Gülich J. *Kreiselpumpen: Handbuch für Entwicklung, Anlagenplanung und Betrieb*, 2nd Edition. Berlin, Germany: Springer-Verlag, 2004.
9. Chambers S, Bartlett R, Ceccio S. Determination of the in vivo cavitation nuclei characteristics of blood. *ASAIO J* 1999;45:541–9.

SNP Best-set Typesetter Ltd.	
Journal Code: AOR	Proofreader: Emily
Article No: 630	Delivery date: 2 September 2008
Page Extent: 7	Copyeditor: Gem

AUTHOR QUERY FORM

Dear Author,

During the preparation of your manuscript for publication, the questions listed below have arisen. Please attend to these matters and return this form with your proof.

Many thanks for your assistance.

Query References	Query	Remark
1	Au: Please note that all instances of "digital particle-image velocimetry" have been changed to **"digital particle image velocimetry"** for consistency throughout the text. Please confirm if this is correct.	
2	Au: The location details **"Saddle Brook, NJ, USA"** has been added for CircuLite. Please confirm if this is correct.	
3	Au: Please supply the manufacturer details of MicroVad pump system.	
4	Au: Please clarify if all instances of "28.000 rpm" should be changed to **"28 000 rpm"**.	
5	Au: Should CAD be written in full? If so, please provide the full form.	
6	Au: Please note that the city **"Canonsburg"** has been added for ANSYS, Inc. Please confirm if this is correct.	